

# $\Xi$ -nucleus potential for $\Xi^-$ quasifree production in the ${}^9\text{Be}(K^-, K^+)$ reaction

Toru Harada<sup>1,2,\*</sup> and Yoshiharu Hirabayashi<sup>3</sup>

<sup>1</sup>*Research Center for Physics and Mathematics,  
Osaka Electro-Communication University,*

*Neyagawa, Osaka, 572-8530, Japan*

<sup>2</sup>*J-PARC Branch, KEK Theory Center,*

*Institute of Particle and Nuclear Studies,*

*High Energy Accelerator Research Organization (KEK),*

*203-1, Shirakata, Tokai, Ibaraki, 319-1106, Japan*

<sup>3</sup>*Information Initiative Center, Hokkaido University, Sapporo, 060-0811, Japan*

(Dated: January 8, 2021)

## Abstract

We study phenomenologically a  $\Xi^-$  production spectrum of the  ${}^9\text{Be}(K^-, K^+)$  reaction at 1.8 GeV/c within the distorted-wave impulse approximation using the optimal Fermi-averaged  $K^-p \rightarrow K^+\Xi^-$  amplitude. We attempt to clarify properties of a  $\Xi$ -nucleus potential for  $\Xi^-$ - ${}^8\text{Li}$ , comparing the calculated spectrum with the data of the BNL-E906 experiment. The results show a weak attraction in the  $\Xi$ -nucleus potential for  $\Xi^-$ - ${}^8\text{Li}$ , which can sufficiently explain the data in the  $\Xi^-$  quasifree region. The strength of  $V_0^\Xi = -17 \pm 6$  MeV is favored within the Woods-Saxon potential, accompanied by the reasonable absorption of  $W_0^\Xi = -5$  MeV for  $\Xi^-p \rightarrow \Xi^0n$ ,  $\Lambda\Lambda$  transitions in nuclear medium. It is difficult to determine the value of  $W_0^\Xi$  from the data due to the insufficient resolution of 14.7 MeV FWHM. The energy dependence of the Fermi-averaged  $K^-p \rightarrow K^+\Xi^-$  amplitude is also confirmed by this analysis, and its importance in the nuclear  $(K^-, K^+)$  reaction is emphasized.

PACS numbers: 21.80.+a, 24.10.Eq, 25.80.Hp, 27.20.+n

---

\*Electronic address: harada@osakac.ac.jp

## I. INTRODUCTION

Recently, Nakazawa *et al.* [1] reported the first evidence of a bound state of the  $\Xi^-$ - $^{14}\text{N}$  system which was identified by the “KISO” event in the KEK-E373 experiment. This result supports that the  $\Xi$ -nucleus potential has a weak attraction of  $V_{\Xi} \simeq -14$  MeV in the Wood-Saxon (WS) potential, as suggested by previous analyses [2–4]. However, there still remains an uncertainty about the nature of the  $S = -2$  dynamics caused by  $\Xi N$  interaction and  $\Xi N$ - $\Lambda\Lambda$  coupling in nuclei due to the limit to the available data. More experimental information is needed for the understanding of  $\Xi$  hypernuclei. Recently, Nagae *et al.* [5] have performed an accurate observation of the  $\Xi^-$  production spectrum in double-charge exchange reactions ( $K^-, K^+$ ) on  $^{12}\text{C}$  targets at 1.8 GeV/ $c$  in the J-PARC E05 experiment, and their analysis is now ongoing. The double-charge exchange reactions such as ( $K^-, K^+$ ) on nuclear targets provide to produce neutron-rich  $\Xi$  hypernuclei, e. g., the neutron excess of  $(N - Z)/(N + Z) = 0.25$  for a  $\Xi^-$ - $^8\text{Li}$  system, which is populated on  $^9\text{Be}$ . The behavior of the  $\Xi^-$  in the neutron-excess environment is strongly connected with the nature of neutron stars [6] in which the baryon fraction is found to depend on properties of hypernuclear potentials [7].

Kohno [8] examined theoretically  $\Xi^-$  production spectra for the quasifree (QF) interaction region in the ( $K^-, K^+$ ) reactions on  $^9\text{Be}$  and  $^{12}\text{C}$  targets in the semiclassical distorted wave method, using the  $\Xi$ -nucleus potential derived from the next-to-leading order (NLO) in chiral effective field theory. However, it has shown that the calculated  $\Xi^-$  QF spectrum on  $^9\text{Be}$  seems to be insufficient to reproduce the experimental data, so that quantitative information on the  $\Xi$ -nucleus potential for  $\Xi^-$ - $^8\text{Li}$  ( $^9_{\Xi^-}\text{He}$ ) may be unreliable.

In this paper, we investigate phenomenologically the  $\Xi^-$  QF spectrum produced via the  $^9\text{Be}(K^-, K^+)$  reaction at 1.8 GeV/ $c$  in order to extract valuable information on the  $\Xi$ -nucleus (optical) potential for the  $\Xi^-$ - $^8\text{Li}$  system from the data of the BNL-E906 experiment [8, 9]. We attempt to clarify properties of the  $\Xi$ -nucleus potential for  $\Xi^-$ - $^8\text{Li}$  and to understand a mechanism of the  $\Xi^-$  QF spectrum in comparison with the data [9]. Thus we demonstrate the calculated  $\Xi^-$  QF spectrum in the  $^9\text{Be}(K^-, K^+)$  reaction within the distorted-wave impulse approximation (DWIA), taking into account the energy dependence of the  $K^- p \rightarrow K^+ \Xi^-$  amplitude in the optimal Fermi-averaging procedure [10, 11].

## II. CALCULATIONS

### A. Distorted-wave impulse approximation

Let us consider production of  $\Xi$  hypernuclear states in the nuclear ( $K^-$ ,  $K^+$ ) reaction. According to the Green's function method [12] in the DWIA, an inclusive  $K^+$  double-differential laboratory cross section of the  $\Xi^-$  production on a nuclear target with a spin  $J_A$  (its  $z$ -component  $M_A$ ) [13–15] is given by

$$\frac{d^2\sigma}{d\Omega dE} = \frac{1}{[J_A]} \sum_{M_A} S(E) \quad (1)$$

with  $[J_A] = 2J_A + 1$ . The strength function  $S(E)$  is written as

$$S(E) = -\frac{1}{\pi} \text{Im} \sum_{\alpha\alpha'} \int d\mathbf{r} d\mathbf{r}' F_{\Xi}^{\alpha\alpha'\dagger}(\mathbf{r}) G_{\Xi}^{\alpha\alpha'}(E; \mathbf{r}, \mathbf{r}') \times F_{\Xi}^{\alpha\alpha'}(\mathbf{r}'), \quad (2)$$

where  $G_{\Xi}^{\alpha\alpha'}$  is a complete Green's function for a  $\Xi$  hypernuclear system,  $F_{\Xi}^{\alpha}$  is a  $\Xi$  production amplitude defined by

$$F_{\Xi}^{\alpha} = \beta^{\frac{1}{2}} \bar{f}_{K^-p \rightarrow K^+\Xi^-} \chi_{\mathbf{p}_{K^+}}^{(-)*} \chi_{\mathbf{p}_{K^-}}^{(+)} \langle \alpha | \hat{\psi}_p | \Psi_A \rangle, \quad (3)$$

and  $\alpha$  ( $\alpha'$ ) denotes the complete set of eigenstates for the system. The kinematical factor  $\beta$  denotes the translation from a two-body  $K^-p$  laboratory system to a  $K^-$ -nucleus laboratory system.  $\bar{f}_{K^-p \rightarrow K^+\Xi^-}$  is a Fermi-averaged amplitude for the  $K^-p \rightarrow K^+\Xi^-$  reaction in nuclear medium [11, 14, 15].  $\langle \alpha | \hat{\psi}_p | \Psi_A \rangle$  is a hole-state wave function for a struck proton in the target.  $\chi_{\mathbf{p}_{K^+}}^{(-)}$  and  $\chi_{\mathbf{p}_{K^-}}^{(+)}$  are distorted waves for outgoing  $K^+$  and incoming  $K^-$  mesons, respectively. The laboratory energy and momentum transfers are  $\omega = E_{K^-} - E_{K^+}$  and  $\mathbf{q} = \mathbf{p}_{K^-} - \mathbf{p}_{K^+}$ , respectively;  $E_{K^+}$  and  $\mathbf{p}_{K^+}$  ( $E_{K^-}$  and  $\mathbf{p}_{K^-}$ ) denote an energy and a momentum of the outgoing  $K^+$  (incoming  $K^-$ ), respectively.

Due to a high momentum transfer  $q \simeq 390\text{--}600$  MeV/ $c$  in the nuclear ( $K^-$ ,  $K^+$ ) reaction for  $K^+$  forward-direction angles of  $\theta_{\text{lab}} = 1.5^\circ\text{--}8.5^\circ$  at  $p_{K^-} = 1.8$  GeV/ $c$ , we simplify the computational procedure for  $\chi_{\mathbf{p}_{K^+}}^{(-)}$  and  $\chi_{\mathbf{p}_{K^-}}^{(+)}$ , using the eikonal approximation [15]. To reduce ambiguities in the distorted-waves, we adopt the same parameters used in calculations for the  $\Lambda$  and  $\Sigma^-$  QF spectra in nuclear ( $\pi^\pm$ ,  $K^+$ ) and ( $K^-$ ,  $\pi^\pm$ ) reactions [11, 16, 17]. Here we used the total cross sections of  $\sigma_{K^-} = 28.9$  mb for the  $K^-N$  scattering and  $\sigma_{K^+} = 19.4$

mb for the  $K^+N$  scattering, and  $\alpha_{K^-} = \alpha_{K^+} = 0$ , as the distortion parameters. We also took into account the recoil effects, which are very important to estimate the hypernuclear production cross section for a light nuclear system [18], leading to an effective momentum transfer having  $q_{\text{eff}} \simeq (1 - 1/A)q \simeq 0.80q$  for  $A = 9$ .

Recently, the authors [10] have found the strong energy dependence of the  $K^-p \rightarrow K^+\Xi^-$  reaction in the nuclear medium, together with the angular dependence for  $\theta_{\text{lab}}$ . Therefore, we emphasize that such behavior of  $\bar{f}_{K^-p \rightarrow K^+\Xi^-}$  plays a significant role in explaining the shape of the spectrum in the nuclear ( $K^-, K^+$ ) reaction [10] as well as those in the nuclear ( $\pi^\pm, K^+$ ) reactions [11, 16, 17]. Because  $\bar{f}_{K^-p \rightarrow K^+\Xi^-}$  provides to modify the spectral shape including the  $\Xi^-$  QF region widely, thus one must extract carefully information concerning the  $\Xi$ -nucleus potential from the data.

## B. Wave functions

For the  ${}^9\text{Be}$  target, the single-particle (s. p.) description of protons is assumed for simplicity. We simulate the calculated results of the s. p. energies of the nucleons and the root-mean-square (rms) radius of  $\langle r_N^2 \rangle^{1/2}$  for their wave functions in the linear combination of atomic orbits (LCAO) models [19] which well describe the ground state of  ${}^9\text{Be}(3/2_{\text{g.s.}}^-; T = 1/2)$  as  $\alpha + \alpha + n$  clusters. Thus we compute the s. p. wave functions for the protons in  $0p$  and  $0s$ , using the WS potential with  $R = r_0 A^{1/3}$  and  $a = 0.67$  fm and omitting the spin-orbit potential; the strength parameter of the potential is adjusted to be  $V_0^N = -58.0$  MeV, together with the size parameter of  $R = 1.60 A^{1/3} = 3.33$  fm which may be rather large due to the structure of  $\alpha + \alpha + n$ . Here we obtain the s. p. energies of  $-22$  MeV for  $0p_{1/2}$  and  $-35$  MeV for  $0s_{1/2}$ , which are consistent with the data of the proton separation energies in  ${}^9\text{Be}(p, 2p)$  reactions indicating widths of 8 MeV for  $0p$  and 13 MeV for  $0s$  [20, 21]. The charge radius of  ${}^9\text{Be}(3/2_{\text{g.s.}}^-)$  is estimated to be 2.53 fm, which is in good agreement with the data of  $2.519 \pm 0.012$  fm in electron elastic scatterings on  ${}^9\text{Be}$  [22]. Note that we must tune in the energies of the s. p. states for the protons as well as the matter rms radius of  $\langle r_N^2 \rangle^{1/2}$  for their wave functions, leading to the fact that the shape of the calculated QF spectrum in the ( $K^-, K^+$ ) reaction sufficiently explain the data.

To calculate the  $\Xi^-$  QF spectrum in the nuclear ( $K^-, K^+$ ) spectrum within the DWIA, we use the Green's function method [12], which is one of the most powerful treatments in the

calculation of a spectrum describing not only bound states but also continuum states with an absorptive potential for spreading components. Because non-spin-flip processes seem to dominate in the  $K^-p \rightarrow K^+\Xi^-$  reaction at 1.8 GeV/c [23], hypernuclear configurations of  $[J_C^\pi \otimes j_\Xi^\pi]_{J_B^\pi}$  with  $J_B^\pi = 3/2^+, 5/2^+, 1/2^-, 3/2^-, 5/2^-, 7/2^-, 3/2^-, 5/2^-, \dots$ , are populated in  ${}^9_{\Xi^-}\text{He}$  with  $T_B = 3/2$ ; we take the  ${}^8\text{Li}$  core nucleus states with  $J_C^\pi = 2^+, 1^+, 2^-,$  and  $1^-$  that are given in  $(3/2^- \otimes p_{3/2,1/2}^{-1})_{2^+,1^+}$  and  $(3/2^- \otimes s_{1/2}^{-1})_{2^-,1^-}$  configurations formed by a proton-hole state on  ${}^9\text{Be}(3/2^-_{\text{g.s.}})$ , and the  $\Xi^-$  with  $j_\Xi^\pi = \ell_\Xi \otimes 1/2 = 1/2^+, 3/2^-, 1/2^-, \dots$  that are given in  $\ell_\Xi \leq 15$  being enough to converge in calculations for the  $\Xi^-$  spectrum. Here the components of  $\Xi^0n$  and  $\Lambda\Lambda$  channels are not considered explicitly because the  $\Xi^-p \rightarrow \Xi^0n$ ,  $\Lambda\Lambda$  transition processes may be described as a spreading imaginary potential in  $\Xi$  bound and continuum regions.

### III. $\Xi$ -NUCLEUS POTENTIAL

The  $\Xi$ -nucleus final states are obtained by solving the Schrödinger equation

$$\left[ -\frac{\hbar^2}{2\mu} \nabla^2 + U_\Xi(r) + U_{\text{Coul}}(r) \right] \Psi_\Xi = E \Psi_\Xi, \quad (4)$$

where  $\mu$  is the  $\Xi$ -nucleus reduced mass,  $U_\Xi$  is the  $\Xi$ -nucleus potential, and  $U_{\text{Coul}}$  is the Coulomb potential. The  $\Xi$ -nucleus potential for  $\Xi^-$ - ${}^8\text{Li}$  is given by

$$\begin{aligned} U_\Xi(r) &= V_\Xi(r) + iW_\Xi(E, r) \\ &= [V_0^\Xi + iW_0^\Xi g(E)] f(r) \end{aligned} \quad (5)$$

with the assumption of the WS form

$$f(r) = [1 + \exp \{(r - R)/a\}]^{-1}, \quad (6)$$

where  $R = r_0 A_{\text{core}}^{1/3}$  and  $a$  denote a radius and a diffuseness of the potential, respectively.  $V_0^\Xi$  is a strength parameter for the real part of the potential;  $W_0^\Xi$  is a strength parameter for the imaginary part of the potential, which denotes the  $\Xi^-$  absorption processes including the  $\Xi^-p \rightarrow \Xi^0n$ ,  $\Lambda\Lambda$  reactions.  $g(E)$  is an energy-dependent function which increases linearly from 0.0 at  $E = E_{\text{th}}(\Lambda)$  to 1.0 at  $E = 20$  MeV with respect to  $\Xi^-$  threshold, as often used in nuclear optical models [24], where  $E_{\text{th}}(\Lambda) = -23.3$  MeV corresponds to the  $\Lambda$  emitted threshold.

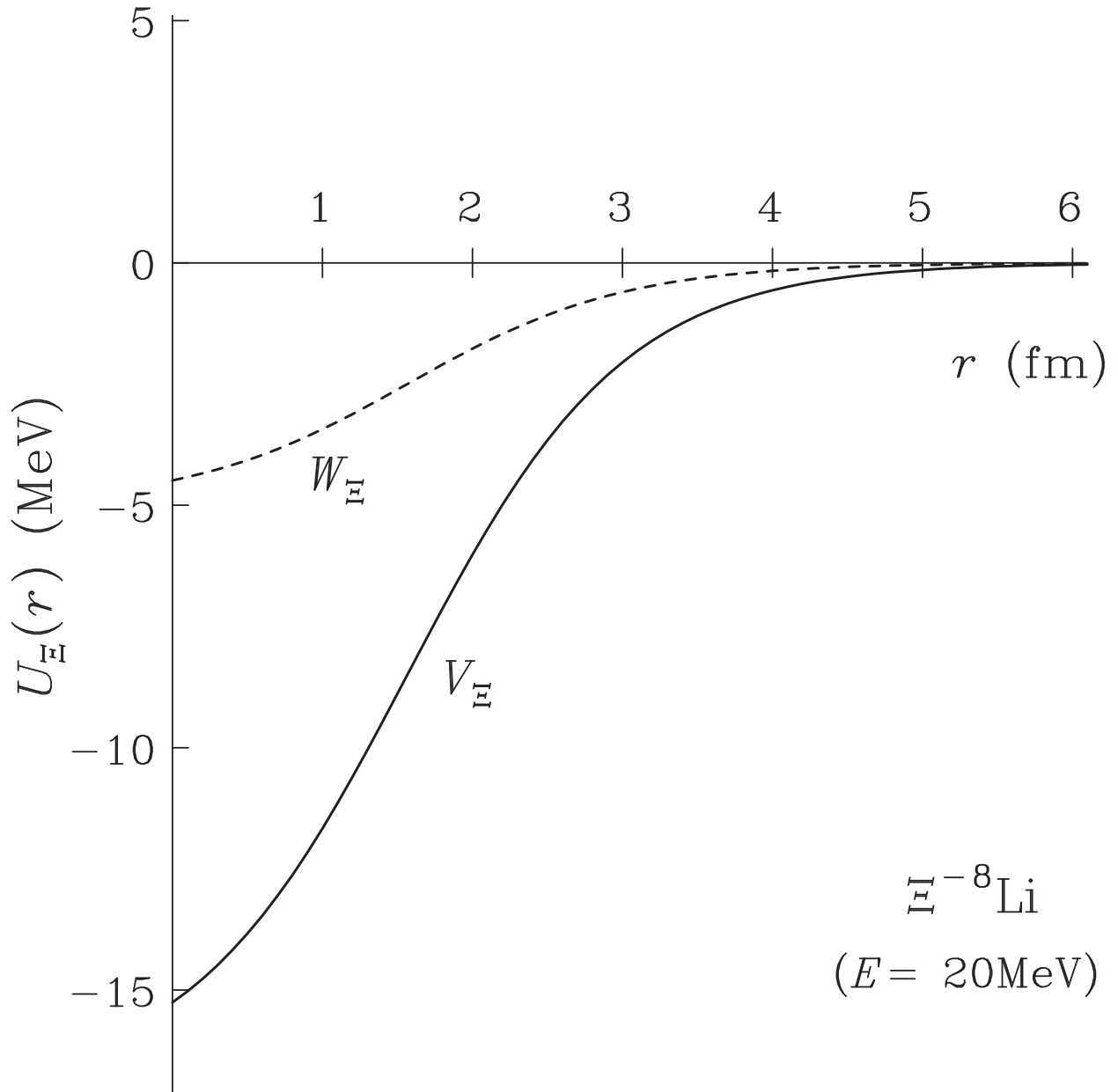


FIG. 1: Real and imaginary parts of the  $\Xi$ -nucleus potential  $U_{\Xi}$  for  $\Xi^{-}$ - ${}^8\text{Li}$  at the energy  $E = 20$  MeV, as a function of the distance between the  $\Xi^{-}$  and the  ${}^8\text{Li}$  nucleus. Solid and dashed curves denote the calculated values for  $V_0^{\Xi} = -17$  MeV and for  $W_0^{\Xi} = -5$  MeV in the WS form, respectively, using  $R = r_0 A_{\text{core}}^{1/3} = 1.57$  fm where  $r_0 = 0.783$  fm and  $a = 0.722$  fm.

The ground state of  ${}^8\text{Li}(2_{\text{g.s.}}^+)$  has a bound state at the neutron binding energy of  $B_n = 2.03$  MeV with respect to the  $n + {}^7\text{Li}_{\text{g.s.}}$  threshold [20]; the matter rms radius of  $\langle r_m^2 \rangle^{1/2} = 2.39 \pm 0.06$  fm is observed experimentally. Thus the appropriate parameters of  $(r_0, a)$  in Eq. (6) must be used, as we shall mention below.

To determine the parameters of  $(r_0, a)$  for the nuclear core in the WS form, we adopt a folding-model potential obtained by convoluting the nuclear one-body density for  ${}^8\text{Li}$  with a two-body  $\Xi^- N$  force. We assume the s.p. density of the spherical shell model for simplicity; the modified harmonic oscillator (MHO) model is used in a systematic description of a size and a density distribution for Li isotopes with  $A = 6-9$  [25]. For  ${}^8\text{Li}(2_{\text{g.s.}}^+)$ , we choose carefully the MHO size parameters of  $b_s = 1.42$  fm and  $b_p = 1.95$  fm with center-of-mass and nucleon-size corrections, adjusting the matter rms radius of  $\langle r_m^2 \rangle^{1/2} = 2.39$  fm [25]. Following to the procedure in Ref. [17], we use the WS form with the parameters of  $(r_0, a)$  adjusted to give a best least-squares fit to the radial shape of the form factor obtained by folding a gaussian range of  $a_{\Xi N} = 1.2$  fm into the matter MHO density distribution [17]. The parameters of the resultant WS form in Eq. (6) are  $r_0 = 0.783$  fm,  $a = 0.722$  fm, and  $R = r_0 A_{\text{core}}^{1/3} = 1.57$  fm, which reproduce the radial shape of the form factor very well; the rms radius of the potential denotes

$$\langle r^2 \rangle_V^{1/2} = \left[ \int r^2 V_{\Xi}(r) dr / \int V_{\Xi}(r) dr \right]^{1/2} = 2.81 \text{ fm}. \quad (7)$$

On the other hand, the spreading imaginary parts of  $W_0^{\Xi}$  may represent complicated continuum states of  ${}^9_{\Lambda\Lambda}\text{He}^*$ ,  ${}^9_{\Xi^-}\text{He}^*$ , and  ${}^9_{\Xi^0}\text{He}^*$ . Considering the states of  ${}^7\text{He}(3/2_{\text{g.s.}}^-)$  located at  $E_{\text{ex}} = 0.45$  MeV above the  $n + {}^6\text{He}$  threshold [20], we have the  $\Lambda$  emitted threshold corresponding to the  $\Lambda + {}^8_{\Lambda}\text{He}$  threshold for the  $\Xi^- p \rightarrow \Lambda\Lambda$  transition. The threshold-energy difference between  $\Xi^-$ - ${}^8\text{Li}$  and  $\Lambda$ - ${}^8_{\Lambda}\text{He}$  channels accounts for  $\Delta M = M({}^8\text{Li}) + m_{\Xi^-} - M({}^8_{\Lambda}\text{He}) - m_{\Lambda} = 23.3$  MeV, where  $M({}^8\text{Li}) = 7471.4$  MeV and  $M({}^8_{\Lambda}\text{He}) = 7654.1$  MeV. For the  $\Xi^- p \rightarrow \Xi^0 n$  transition, the  $\Xi^0$  emitted threshold for  $\Xi^0$ - ${}^8\text{He}$  is located at  $E = 4.3$  MeV above the  $\Xi^-$ - ${}^8\text{Li}$  threshold. The spin-orbit potential for  $\Xi^-$  is also considered to denote a term of  $V_{\text{so}}^{\Xi}(1/r)[df(r)/dr]\boldsymbol{\sigma} \cdot \mathbf{L}$ , where  $V_{\text{so}}^{\Xi} \simeq \frac{1}{10} V_{\text{so}}^N \simeq 2$  MeV [26]. For  $U_{\text{Coul}}$ , we use the attractive Coulomb potential with the uniform distribution of a charged sphere where  $Z = 3$  for  $\Xi^-$ - ${}^8\text{Li}$ .

We attempt to determine the strength parameters of  $V_0^{\Xi}$  and  $W_0^{\Xi}$  in Eq. (5) phenomenologically in comparison with the data of the  ${}^9\text{Be}(K^-, K^+)$  reaction. Figure 1 shows the real

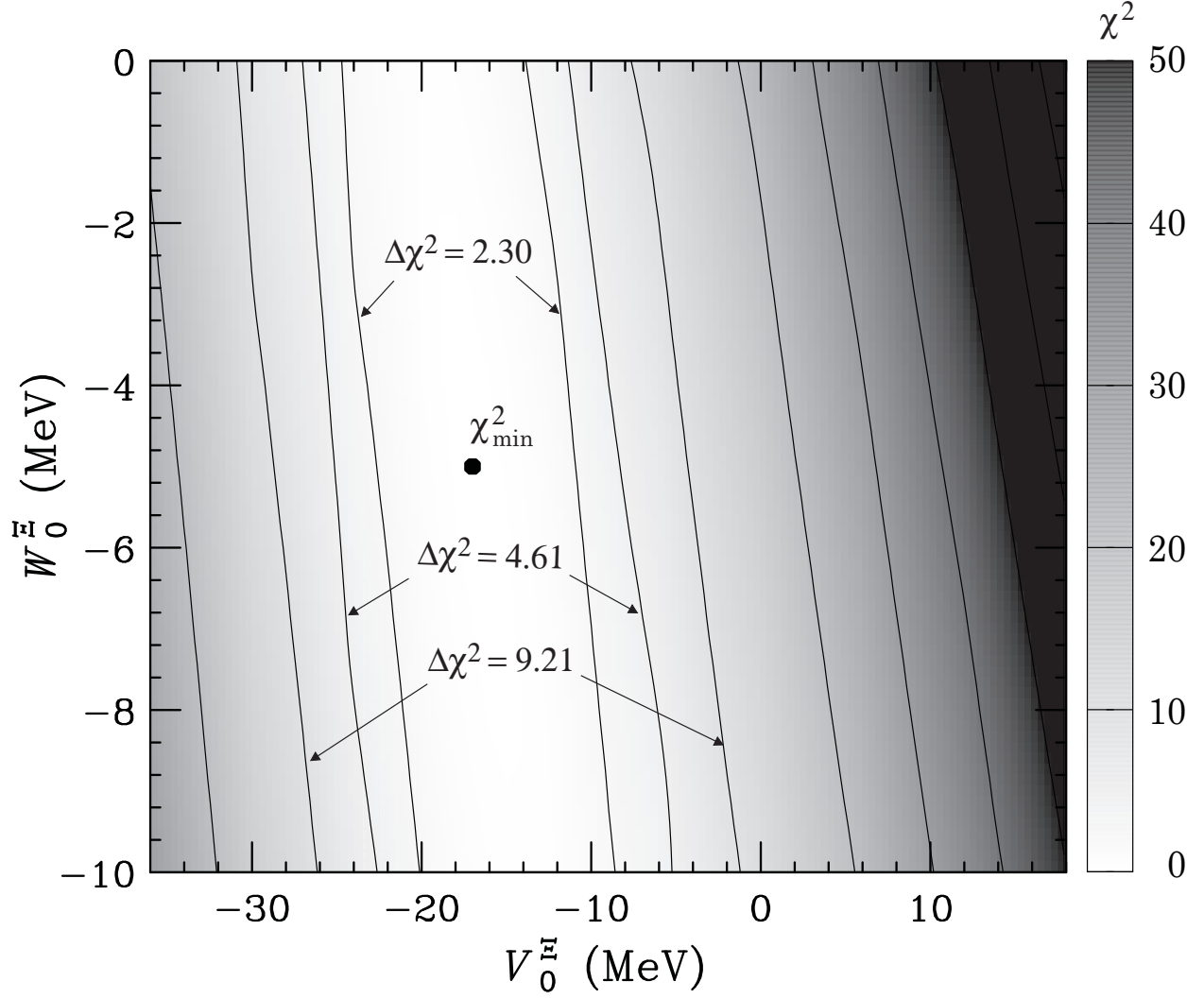


FIG. 2: Contour plots of the  $\chi^2$ -value distribution in the  $\{V_0^\Xi, W_0^\Xi\}$  plane from fitting to the average cross section of  $\bar{\sigma}_{1.5^\circ-8.5^\circ}$  in the  ${}^9\text{Be}(K^-, K^+)$  reaction at  $p_{K^-} = 1.8 \text{ GeV}/c$ . A solid circle denotes the minimum position of  $\chi_{\min}^2 = 15.2$  at  $(V_0^\Xi, W_0^\Xi) = (-17 \text{ MeV}, -5 \text{ MeV})$  with  $f_s = 0.940$ . The solid lines labeled by  $\Delta\chi^2 = 2.30, 4.61,$  and  $9.21$  correspond to 68%, 90%, and 99% confidence levels for 2 parameters, respectively.

and imaginary parts of the  $\Xi$ -nucleus potential for  $\Xi^-$ - ${}^8\text{Li}$ , choosing the reasonable strengths of  $V_0^\Xi = -17 \text{ MeV}$  and  $-5 \text{ MeV}$ , as we will discuss it in Sect. IV.



TABLE I: The  $\chi^2$ -fitting for various strength parameters,  $V_0^\Xi$  and  $W_0^\Xi$ , in the WS potential with  $r_0 = 0.738$  fm and  $a = 0.722$  fm for  $\Xi^-$ - $^8\text{Li}$ . The value of  $\chi^2/N$  and the renormalization factor  $f_s$  are obtained by comparing the calculated spectrum with the  $N = 17$  data points of the average cross sections of  $\bar{\sigma}_{1.5^\circ-8.5^\circ}$  for  $p_{K^+} = 1.07\text{--}1.39$  GeV/ $c$ . The data were taken from Ref. [9].

$V_0^\Xi$ (MeV)	$W_0^\Xi$ (MeV)	$N = 17$ data points	
		$\chi^2/N$	$f_s$
+12	0	69.8/17	0.988
0	0	37.6/17	0.964
-6	0	26.4/17	0.951
-12	0	18.9/17	0.939
-18	0	15.6/17	0.927
-24	0	16.8/17	0.914
-30	0	22.8/17	0.902
+12	-5	58.3/17	0.999
0	-5	30.7/17	0.975
-6	-5	21.8/17	0.962
-12	-5	16.5/17	0.950
-17	-5	15.2/17	0.940
-18	-5	15.3/17	0.938
-24	-5	18.4/17	0.925
-30	-5	26.1/17	0.913
+12	-10	49.0/17	1.010
0	-10	25.7/17	0.985
-6	-10	18.9/17	0.973
-12	-10	15.6/17	0.961
-18	-10	16.3/17	0.948
-24	-10	21.1/17	0.936
-30	-10	30.4/17	0.923

## IV. RESULTS

### A. $\chi^2$ fitting

Tamagawa *et al.* (BNL-E906 collaboration) reported the experimental data of the  $\Xi^-$  QF spectra for the  $K^+$  forward-direction angles of  $\theta_{\text{lab}} = 1.5^\circ\text{--}8.5^\circ$  in the  ${}^9\text{Be}(K^-, K^+)$  reactions at the incident  $K^-$  momentum of  $p_{K^-} = 1.8 \text{ GeV}/c$  [9]. The average cross section  $\bar{\sigma}_{1.5^\circ\text{--}8.5^\circ}$  in the laboratory frame was obtained by

$$\bar{\sigma}_{1.5^\circ\text{--}8.5^\circ} \equiv \int_{\theta_{\text{lab}}=1.5^\circ}^{\theta_{\text{lab}}=8.5^\circ} \left( \frac{d^2\sigma}{dp_{K^+}d\Omega_{K^+}} \right) d\Omega / \int_{\theta_{\text{lab}}=1.5^\circ}^{\theta_{\text{lab}}=8.5^\circ} d\Omega \quad (8)$$

with the detector resolution of 14.7 MeV FWHM [9]. The strength parameters of  $V_0^\Xi$  and  $W_0^\Xi$  in Eq. (5) should be adjusted appropriately to reproduce the data of  $\bar{\sigma}_{1.5^\circ\text{--}8.5^\circ}$ .

We consider the  $\Xi^-$  QF spectrum for  $\Xi^-$ - ${}^8\text{Li}$  hypernuclear states with  $J_B^\pi, T_B = 3/2$ , using the Green's function method [12], in order to be compared with the data of the  ${}^9\text{Be}(K^-, K^+)$  reaction at the BNL-E906 experiment [9]. Calculating the spectra for  $\theta_{\text{lab}} = 1.5^\circ\text{--}8.5^\circ$ , we estimate the average cross section for the corresponding  $\bar{\sigma}_{1.5^\circ\text{--}8.5^\circ}$  in Eq. (8). To make a fit to the spectral shape of the data, we will introduce a renormalization factor of  $f_s$  into the absolute value of the calculated spectrum because the eikonal distortion and the amplitude of  $\bar{f}_{K^-p \rightarrow K^+\Xi^-}$  would have some ambiguities [10, 15]. The detector resolution of 14.7 MeV FWHM is also taken into account. We obtain the values of  $\chi^2$  for fits to the data points of  $N = 17$  in  $p_{K^+} = 1.07\text{--}1.39 \text{ GeV}/c$ , varying the strengths of  $(V_0^\Xi, W_0^\Xi)$  and  $f_s$ ; we assumed the value of  $0.018 \mu\text{b}/\text{sr}/\text{MeV}c^{-1}$  as a constant background. Thus we estimate the average cross section in Eq. (8), calculating the spectra for  $\theta_{\text{lab}} = 1.5^\circ\text{--}8.5^\circ$  in the parameter region of  $V_0^\Xi = (-36)\text{--}(+18) \text{ MeV}$  by a 6 MeV energy step and  $W_0^\Xi = (-10)\text{--}0 \text{ MeV}$  by a 2 MeV energy step. The 1 MeV energy step is taken in the estimation near the  $\chi_{\text{min}}^2$  point.

Figure 2 displays the contour plots of  $\chi^2$ -value distribution for  $\bar{\sigma}_{1.5^\circ\text{--}8.5^\circ}$ . The minimum value of  $\chi^2$  is found to be  $\chi_{\text{min}}^2 = 15.2$  at  $V_0^\Xi = -17 \text{ MeV}$ ,  $W_0^\Xi = -5 \text{ MeV}$ , and  $f_s = 0.940$ , leading to belt-like regions of  $\Delta\chi^2 = 2.30, 4.61, \text{ and } 9.21$  which correspond to 68%, 90%, and 99% confidence levels for 2 parameters, respectively, where  $\Delta\chi^2 \equiv \chi^2 - \chi_{\text{min}}^2$ . We find that the value of  $\chi^2$  is almost insensitive to  $W_0^\Xi$ . This fact implies that the parameter of  $W_0^\Xi$  cannot be determined from the BNL-E906 data due to the insufficient resolution of 14.7 MeV FWHM. Nevertheless, we recognize that the calculated spectrum for  $V_0^\Xi \simeq -17 \text{ MeV}$  seems to be in good agreement with the data when  $W_0^\Xi \simeq -5 \text{ MeV}$ ; it gives the minimum

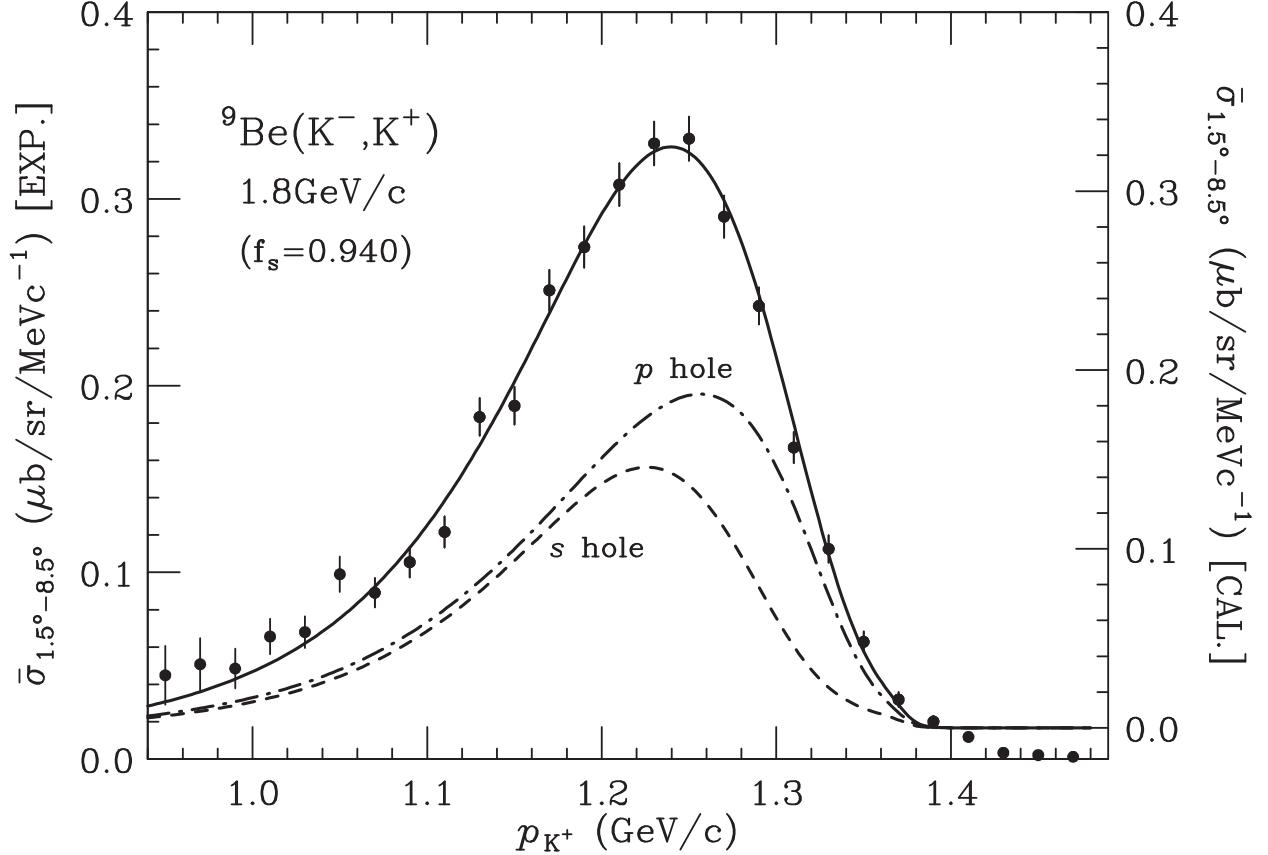


FIG. 3: Calculated spectrum for  $\bar{\sigma}_{1.5^\circ-8.5^\circ}$  in the WS potential with  $V_0^\Xi = -17$  MeV,  $W_0^\Xi = -5$  MeV,  $r_0 = 0.738$  fm, and  $a = 0.722$  fm, together with the data of the  $^9\text{Be}(K^-, K^+)$  reaction at  $p_{\pi^-} = 1.8$  GeV/c [9]. The calculated spectrum is normalized by  $f_s = 0.940$  for fits to the data. Solid, dashed, and dot-dashed curves denote the contributions of total,  $s$ -hole, and  $p$ -hole configurations, respectively. The calculated values are folded with a detector resolution of 14.7 MeV FWHM.

value of  $\chi^2/N = 15.2/17 = 0.89$ , and the standard deviation of  $\sigma \simeq 6$  MeV. In Table I, we list the reduced  $\chi^2$  values of  $\chi^2/N$  in calculations when  $V_0^\Xi = -30, -24, -18, -12, -6, 0,$  and  $+12$  MeV, and  $W_0^\Xi = -10, -5,$  and  $0$  MeV, comparing the calculated spectra with the data. Note that the absolute values of the calculated cross section can explain the magnitude of the data, as seen by  $f_s \simeq 0.9-1.0$ .

Figure 3 shows the absolute values of the calculated spectrum for  $\bar{\sigma}_{1.5^\circ-8.5^\circ}$  in the best-fit calculation, comparing them with the data of the BNL-E906 experiment at  $p_{K^+} = 1.07-1.39$  GeV/c. We recognize that an attraction in the  $\Xi^-$ - $^8\text{Li}$  potential is needed to reproduce the data. The contribution of  $p$ -hole configurations is larger than that of  $s$ -hole configurations in the  $\Xi^-$  QF region of  $p_{K^+} = 1.2-1.4$  GeV/c, whereas the former is similar to the latter

TABLE II: Binding energies  $B_{\Xi^-}$  and widths  $\Gamma_{\Xi^-}$  of the  $\Xi^-$ -nucleus ( $n\ell$ ) bound states for  $\Xi^-$ - $^8\text{Li}$  ( $^9_{\Xi^-}\text{He}$ ). The strengths of  $V_0^{\Xi} = -17$  MeV and  $W_0^{\Xi} = -2.5$  (-1.5) MeV are used in the WS potential for the  $\Xi^-$  bound region. These values are estimated in combination with the  $\Xi$ -nucleus potential  $U_{\Xi} = V_{\Xi} + iW_{\Xi}$  and the Coulomb potential  $U_{\text{Coul}}$ .

$(n\ell)$	$V_{\Xi} + U_{\text{Coul}} + iW_{\Xi}$			$V_{\Xi} + U_{\text{Coul}}$		$V_{\Xi}$		$U_{\text{Coul}}$	
	$-B_{\Xi^-}$ (MeV)	$\Gamma_{\Xi^-}$ (MeV)	rms (fm)	$-B_{\Xi^-}$ (MeV)	rms (fm)	$-B_{\Xi^-}$ (MeV)	rms (fm)	$-B_{\Xi^-}$ (MeV)	rms (fm)
$W_0^{\Xi} = -2.5$ MeV									
1S	-1.851	1.118	3.95	-1.897	3.96	-0.475	5.56	-0.255	14.6
2S	-0.122	$1.3 \times 10^{-2}$	29.3	-0.122	29.5	—	—	-0.066	53.4
2P	-0.068	$3.1 \times 10^{-4}$	43.4	-0.068	43.4	—	—	-0.067	44.0
$W_0^{\Xi} = -1.5$ MeV									
1S	-1.880	0.669	3.95						
2S	-0.122	$8.0 \times 10^{-3}$	29.4						
2P	-0.068	$1.9 \times 10^{-4}$	43.4						

in the region of  $p_{K^+} < 1.2$  GeV/ $c$  where the recoil momentum grows into  $q > 540$  MeV/ $c$ . Consequently, we confirm that the  $\Xi$  potential for  $\Xi^-$ - $^8\text{Li}$  has a weak attraction in the real part of the WS potential with  $r_0 = 0.738$  fm and  $a = 0.722$  fm;

$$V_0^{\Xi} = -17 \pm 6 \text{ MeV} \quad \text{for } W_0^{\Xi} = -5 \text{ MeV}. \quad (9)$$

This potential provides the ability to explain the  $^9\text{Be}(K^-, K^+)$  data at the BNL-E906 experiment. Several authors [2, 3] attempted to determine the values of  $V_0^{\Xi}$  for fits to the shape and magnitude of the  $\Xi^-$  QF spectra from the data of the  $^{12}\text{C}(K^-, K^+)$  reaction [3]. They suggested that the  $\Xi$ -nucleus potential has a weak attraction of  $V_0^{\Xi} \simeq -14$  MeV in the WS potential. It is shown that the results of Eq. (9) in our analysis are considerably consistent with the results of the previous studies [2, 3].

## B. $\Xi^-$ -nucleus bound states

In Table II, we show the numerical results of binding energies and widths of the  $\Xi^-$ -nucleus ( $n\ell$ ) bound states for  $\Xi^-$ - $^8\text{Li}$ , where ( $n\ell$ ) denote the principal and angular momentum quantum numbers for the relative motion between  $\Xi^-$  and  $^8\text{Li}$ . By solving the Schrödinger equation of Eq. (4) with the WS potential  $U_{\Xi}$  and the finite Coulomb potential  $U_{\text{Coul}}$ , we obtain a complex eigenvalue as a Gamow state,

$$E_{n\ell} = -B_{\Xi^-} - i\frac{\Gamma_{\Xi^-}}{2}, \quad (10)$$

where  $B_{\Xi^-}$  and  $\Gamma_{\Xi^-}$  denote a binding energy and a width of the bound state, respectively. When we use  $V_0^{\Xi} = -17$  MeV in the WS potential, we confirm that there exists a very shallow  $\Xi^-$  ( $1S$ ) bound state due to the weak attraction in the  $\Xi$ -nucleus potential even if the Coulomb potential is switched off; the binding energy accounts for  $B_{\Xi^-}(1S) = 0.475$  MeV and the rms radius of  $\langle r^2 \rangle^{1/2} = 5.56$  fm. When the Coulomb potential is switched on, the binding energy is significantly shifted downward in comparison with the corresponding Coulomb eigenstate, as seen in Table II. Thus this state is often regarded as a ‘‘Coulomb-assisted’’  $\Xi^-$ -nucleus bound state;  $B_{\Xi^-}(1S) = 1.90$  MeV and  $\langle r^2 \rangle^{1/2} = 3.96$  fm.

A  $\Xi^-$  hyperon bound in nuclei must be absorbed by strong interaction via the  $\Xi^-p \rightarrow \Lambda\Lambda$  conversion process. To estimate the width of the  $\Xi^-$  bound state, we assume the value of  $W_0^{\Xi} = -2.5$  MeV, which corresponds to the strength of  $W_{\Xi}(E)$  at the  $\Xi^-$  threshold ( $E = 0.0$  MeV). Thus we obtain the width of  $\Gamma_{\Xi^-}(1S) = 1.12$  MeV, together with  $B_{\Xi^-}(1S) = 1.85$  MeV. When we use  $W_0^{\Xi} = -1.5$  MeV arising from the  $\Xi^-p \rightarrow \Lambda\Lambda$  conversion in the  $\Xi N$  NLO potential [28, 29], we obtain  $\Gamma_{\Xi^-}(1S) = 0.669$  MeV and  $B_{\Xi^-}(1S) = 1.88$  MeV. (See also Sect. VB.)

## V. DISCUSSION

### A. Effects of the real part of the $\Xi$ -nucleus potential

To see effects of the attraction in the  $\Xi$ -nucleus potential for  $\Xi^-$ - $^8\text{Li}$ , we discuss the shapes and magnitudes of the calculated spectra. Figure 4 shows the absolute values of the calculated spectra for  $\bar{\sigma}_{1.5^\circ-8.5^\circ}$  in the  $\Xi^-$  QF region, using various strengths of  $V_0^{\Xi}$ . We find that the shape and magnitude of the calculated spectrum are considerably sensitive to the

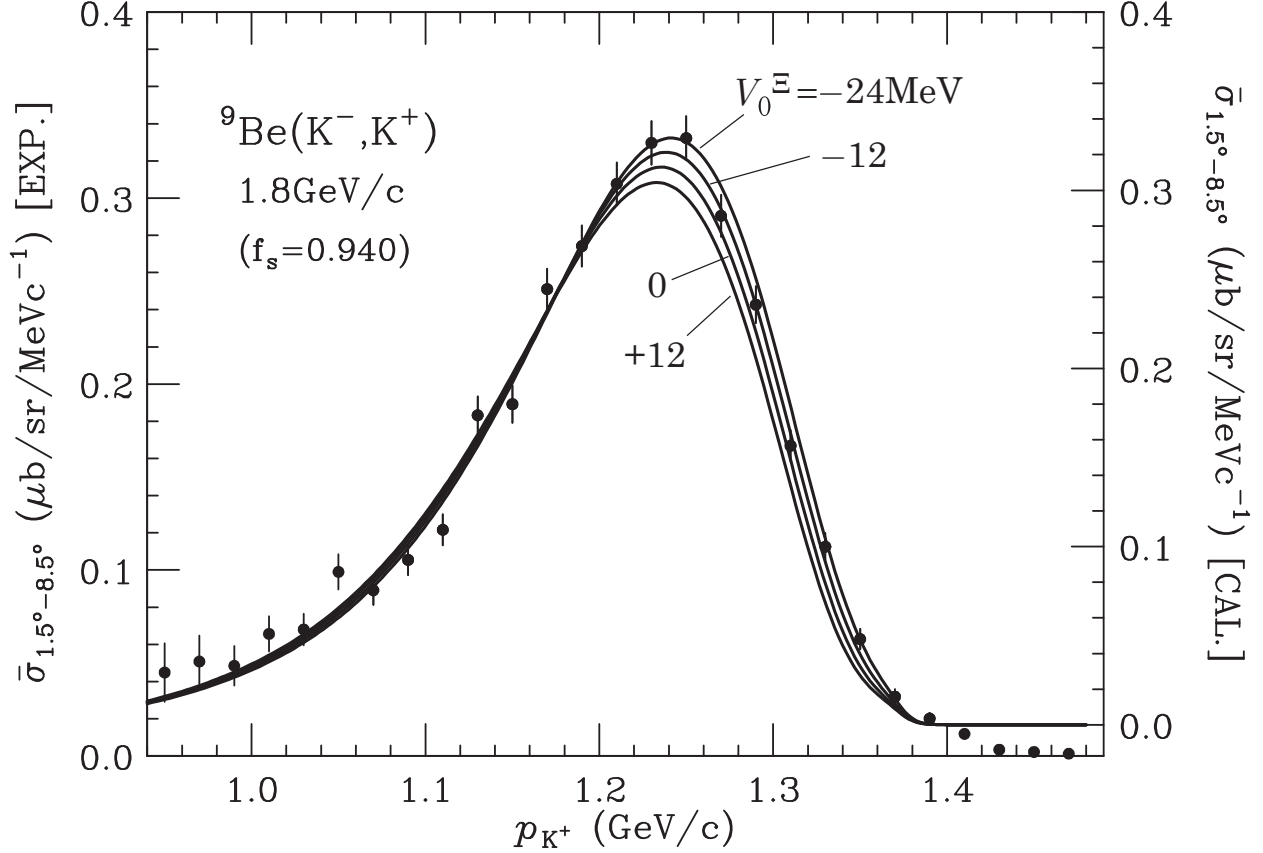


FIG. 4: Shapes and magnitudes of the calculated spectra for  $\bar{\sigma}_{1.5^\circ-8.5^\circ}$  in the  $^9\text{Be}(K^-, K^+)$  reaction at  $p_{K^-} = 1.80$  GeV/c, depending on the strengths of  $V_0^\Xi = -24, -12, 0,$  and  $+12$  MeV in the WS potential with  $W_0^\Xi = -5$  MeV. The spectra are folded with a detector resolution of 14.7 MeV FWHM.

value of  $V_0^\Xi$ . This confirms that the value of  $\chi^2/N$  is significantly changed by  $V_0^\Xi$ . The peak position of the QF spectrum is scarcely shifted downward for  $p_{K^+}$ , as  $V_0^\Xi$  changes from  $-24$  MeV to  $+12$  MeV, whereas the magnitude of this peak is slightly reduced by 8.4%. There appears the difference between the spectra of  $V_0^\Xi = (-24)-(+12)$  MeV in the momentum region of  $p_{K^+} > 1.2$  GeV/c, corresponding to the region of lower energies  $E < 140$  MeV. On the other hand, the shapes and magnitudes of the spectra with  $V_0^\Xi = (-24)-(+12)$  MeV become similar to each other in the region of higher energies  $E > 140$  MeV ( $p_{K^+} < 1.2$  GeV/c).

## B. Validity of the imaginary part of the $\Xi$ -nucleus potential

In Sect. IV A, we have found that the shapes and magnitudes of the calculated spectra are not so sensitive to the value of  $W_0^\Xi$  when we change  $W_0^\Xi = (-10)-0$  MeV in the imaginary part of the  $\Xi$ -nucleus potential. This reason is because a mask of  $W_0^\Xi$  is inevitable due to the insufficient resolution of 14.7 MeV FWHM. Thus we recognize that it is difficult to determine the value of  $W_0^\Xi$ .

According to the procedure by Gal, Toker, and Alexander [27], we examine theoretically an appropriate parameter for  $W_0^\Xi$  from a viewpoint of the first order optical ( $t\rho$ ) potential,

$$U_\Xi^{(1)}(r) = t_{\Xi^-p}\rho_p(r) + t_{\Xi^-n}\rho_n(r) \quad (11)$$

in terms of the effective two-body  $\Xi N$  elastic  $t_{\Xi N}$  scattering matrices in the laboratory frame, where  $\rho_{p,n}(r)$  are the proton and neutron densities of the core nucleus. By the optical theorem  $4\pi\text{Im}f_{\Xi N} = k_\Xi\sigma_{\text{tot}}$  and considering collisions of zero energy  $\Xi$  with bound nucleons, we obtain the imaginary part  $W_\Xi^{(1)}$  of the optical potential involving the  $\Xi^-p \rightarrow \Xi^0n, \Lambda\Lambda$  conversion, which is given by

$$W_\Xi^{(1)}(r) = -\langle v_{\Xi^-p}\sigma(\Xi^-p \rightarrow \Xi^0n, \Lambda\Lambda) \rangle \\ \times \rho_p(r)/2, \quad (12)$$

where  $v$  is the relative velocity of a  $\Xi^-p$  pair, and  $\langle \dots \rangle$  indicates nuclear medium corrections to the free space value of  $v\sigma$  arising from Fermi averaging, binding effects, and Pauli principle, etc. The cross section is well approximated up to 300 MeV/ $c$  in the laboratory system by the form

$$v_{\Xi^-p}\sigma = (v_{\Xi^-p}\sigma)_0/(1 + \alpha v), \quad (13)$$

with the two representative parametrization of  $(v_{\Xi^-p}\sigma)_0 = 25$  mb and  $\alpha = 18$  for the  $\Xi^-p \rightarrow \Xi^0n, \Lambda\Lambda$  reactions, fitting to  $v_{\Xi^-p}\sigma$  which are given by the  $\Xi N$  NLO potential [28, 29]. Taking into account the closure assumption and nuclear medium corrections [27], we obtain  $\langle v_{\Xi^-p}\sigma \rangle = 7.02$  mb within the Fermi gas model. Using the relation between  $\langle v\sigma \rangle$  and  $\text{Im}b$ , where  $b$  is the effective parameter of a complex scattering length for  $\Xi^-p$ , we roughly estimate

$$\text{Im}b = \mu\langle v\sigma \rangle/8\pi = 0.078 \text{ fm}, \quad (14)$$

TABLE III: Comparison of the standard Fermi-averaged differential cross sections  $(d\sigma/d\Omega)_{\text{lab}}^{\text{av}}$  for the  $K^-p \rightarrow K^+\Xi^-$  reaction at  $p_{K^-} = 1.8$  GeV/ $c$  with the differential cross sections  $(d\sigma/d\Omega)_{\text{lab}}^{\text{free}}$  for the  $K^-p \rightarrow K^+\Xi^-$  reaction in free space [10]. The values are in unit of mb/sr.

$\theta_{\text{lab}}$	1°	2°	3°	4°	5°	6°	7°	8°	9°
$(d\sigma/d\Omega)_{\text{lab}}^{\text{av}}$	55.4	54.7	53.5	51.9	50.0	47.8	45.5	43.1	40.7
$(d\sigma/d\Omega)_{\text{lab}}^{\text{free}}$	67.1	65.9	64.1	61.7	58.8	55.6	52.3	49.0	45.8

of which the value corresponds to  $W_0^{\Xi} = -6.2$  MeV in the WS potential. We find that this value is similar to  $W_0^{\Xi} = -5$  MeV for the minimum value of  $\chi_{\text{min}}$ , as shown in Fig. 2. If we replace the momentum distributions of the Fermi gas model by those of the s. p. shell model for the finite nuclei, the results may not change. Therefore, we believe that the  $\Xi^-$ -nucleus potential with  $V_0^{\Xi} = -17$  MeV and  $W_0^{\Xi} = -5$  MeV is appropriate to the study of the  $\Xi^-$  QF spectrum in the  ${}^9\text{Be}(K^-, K^+)$  reaction at  $p_{K^-} = 1.8$  GeV/ $c$ .

Considering the same manner for only the  $\Xi^-p \rightarrow \Lambda\Lambda$  conversion [28, 29], we also obtain  $(v_{\Xi^-p}\sigma)_0 = 4.5$  mb and  $\alpha = 20$ . Thus we estimate  $\text{Im}b = 0.018$  fm, which corresponds to  $W_0^{\Xi} = -1.5$  MeV. Such a small absorption of  $W_0^{\Xi} \simeq -1$  MeV may be acceptable because the  $\Xi^-p \rightarrow \Lambda\Lambda$  coupling is recently predicted to be rather small [8, 30].

### C. Verification of the optimal Fermi-averaged $K^-p \rightarrow K^+\Xi^-$ amplitude

In a previous paper [10], we emphasized the importance of the energy dependence of the  $K^-p \rightarrow K^+\Xi^-$  amplitude of  $\bar{f}_{K^-p \rightarrow K^+\Xi^-}$  arising from the optimal Fermi-averaging procedure [11] in the nuclear  $(K^-, K^+)$  reaction. We discuss the calculated  $\Xi^-$  QF spectra involving the energy dependence of  $\bar{f}_{K^-p \rightarrow K^+\Xi^-}$  in comparison with the data of the  ${}^9\text{Be}(K^-, K^+)$  reaction in the BNL-E906 experiment. To see the importance of the energy dependence of  $\bar{f}_{K^-p \rightarrow K^+\Xi^-}$ , we also estimate the spectrum in the DWIA using the ‘‘standard’’ Fermi-averaged cross section  $(d\sigma/d\Omega)_{\text{lab}}^{\text{av}}$  for the  $K^-p \rightarrow K^+\Xi^-$  reaction, which may be given by

$$\left(\frac{d\sigma}{d\Omega}\right)_{\text{lab}}^{\text{av}} = \int d\mathbf{p}_N \rho(p_N) \left(\frac{d\sigma}{d\Omega}\right)_{\text{lab}}^{\text{free}}, \quad (15)$$

where  $\rho(p_N)$  is a proton momentum distribution in the target nucleus, and  $(d\sigma/d\Omega)_{\text{lab}}^{\text{free}}$  is the differential cross section for the  $K^-p \rightarrow K^+\Xi^-$  reaction in free space. This spectrum



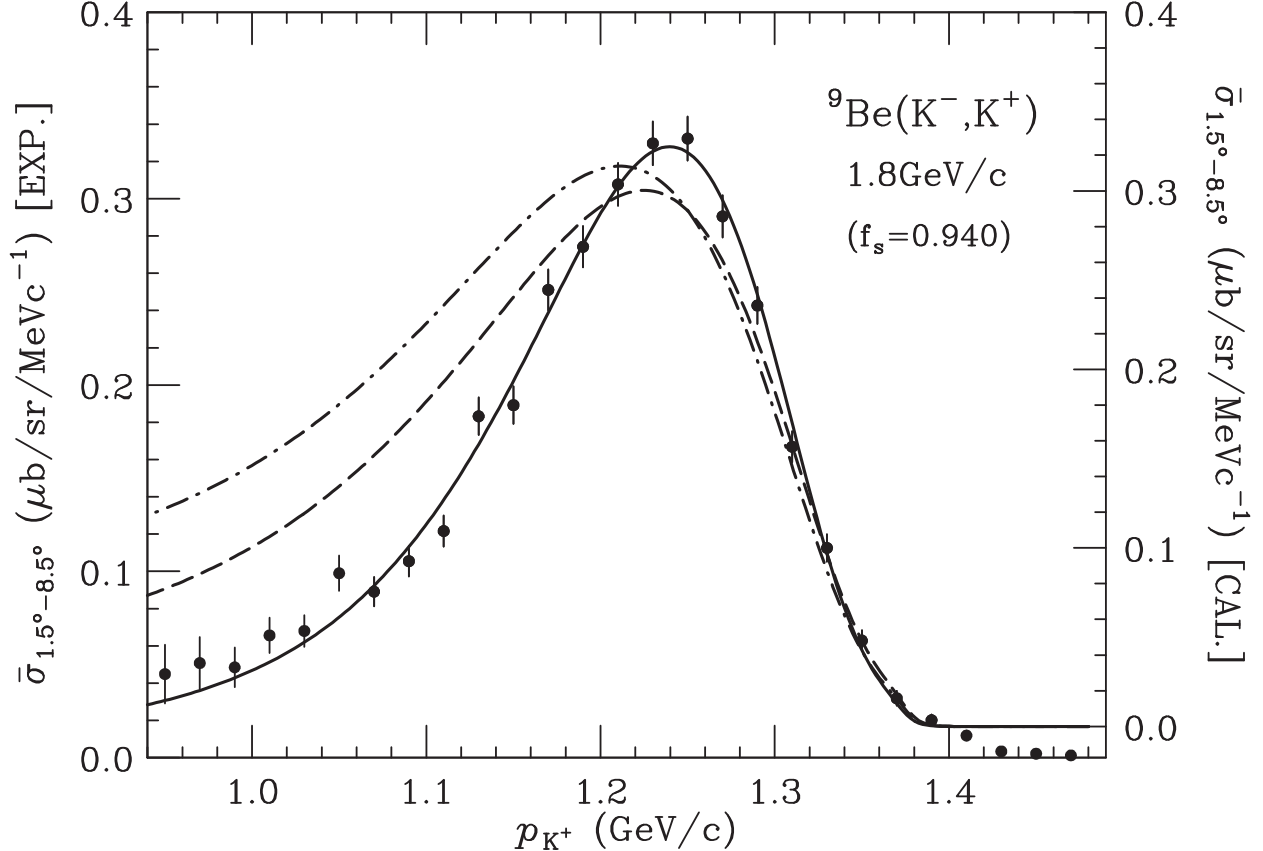


FIG. 5: Comparison of the calculated spectra for  $\bar{\sigma}_{1.5^\circ-8.5^\circ}$  with the data of the  ${}^9\text{Be}(K^-, K^+)$  reaction at  $p_{K^-} = 1.80$  GeV/c [9], using the WS potential with  $V_0^\Xi = -17$  MeV and  $W_0^\Xi = -5$  MeV. Solid and dashed curves denote the spectra obtained by the optimal and standard Fermi-averaged  $K^-p \rightarrow K^+\Xi^-$  amplitudes for  $\bar{f}_{K^-p \rightarrow K^+\Xi^-}$ , respectively. A dot-dashed curve denotes the spectrum obtained by  $\beta(d\sigma/d\Omega)_{\text{lab}}^{\text{av}} = \text{constant}$ . The spectra are folded with a detector resolution of 14.7 MeV FWHM.

is proportional to  $\beta(d\sigma/d\Omega)_{\text{lab}}^{\text{av}}$  indicating the energy dependence of  $\beta$  whereas the value of  $(d\sigma/d\Omega)_{\text{lab}}^{\text{av}}$  at each  $\theta_{\text{lab}}$  becomes constant in Eq. (15). In Table III, we show the calculated values of  $(d\sigma/d\Omega)_{\text{lab}}^{\text{av}}$  and  $(d\sigma/d\Omega)_{\text{lab}}^{\text{free}}$  [10]. Figure 5 displays the calculated  $\Xi^-$  QF spectra obtained by the optimal and standard Fermi-averaged  $K^-p \rightarrow K^+\Xi^-$  amplitudes in the  ${}^9\text{Be}(K^-, K^+)$  reaction at  $p_{K^-} = 1.8$  GeV/c, together with the spectrum obtained by  $\beta(d\sigma/d\Omega)_{\text{lab}}^{\text{av}} = \text{constant}$ , omitting the energy dependence of  $\beta$ . We find that the energy dependence of  $\bar{f}_{K^-p \rightarrow K^+\Xi^-}$  acts on the shape and magnitude of the QF spectrum remarkably, and it makes its width narrower. If we use a constant value for  $\bar{f}_{K^-p \rightarrow K^+\Xi^-}$  in our calculations, the shape and magnitude of the calculated  $\Xi^-$  QF spectrum cannot explain the

data qualitatively. We show clearly that the optimal Fermi averaging for the  $K^-p \rightarrow K^+\Xi^-$  reaction provides a good description of the energy dependence of the  $\Xi^-$  QF spectrum in the nuclear ( $K^-, K^+$ ) reaction [10]. Therefore, we recognize that the optimal Fermi-averaged amplitudes for  $\bar{f}_{K^-p \rightarrow K^+\Xi^-}$  is essential to explain the shape and magnitude of the spectrum including the  $\Xi^-$  QF region with a wide energy range. Thus it is required to extract information concerning the  $\Xi$ -nucleus potential carefully from the data of the experimental spectrum.

## VI. SUMMARY AND CONCLUSION

We have studied phenomenologically the  $\Xi^-$  production spectrum of the  ${}^9\text{Be}(K^-, K^+)$  reaction at 1.8 GeV/ $c$  within the DWIA using the optimal Fermi-averaged  $K^-p \rightarrow K^+\Xi^-$  amplitude. We have attempted to clarify properties of the  $\Xi$ -nucleus potential for  $\Xi^-$ - ${}^8\text{Li}$ , comparing the calculated spectrum with the data of the BNL-E906 experiment. We have performed the  $\chi^2$ -fitting to the  $N = 17$  data points for  $\bar{\sigma}_{1.5^\circ-8.5^\circ}$ , varying the strength parameters of  $V_0^\Xi$  and  $W_0^\Xi$  in the WS potential.

In conclusion, we show the weak attraction in the  $\Xi$ -nucleus potential for  $\Xi^-$ - ${}^8\text{Li}$ , which provides the ability to explain the data for the  $\Xi^-$  QF region in the  ${}^9\text{Be}(K^-, K^+)$  reaction at 1.8 GeV/ $c$ , consistent with analyses for previous experiments [1, 3]. The attraction of  $V_0^\Xi = -17 \pm 6$  MeV is favored within the WS potential, accompanied by the reasonable absorption of  $W_0^\Xi = -5$  MeV for the  $\Xi^-p \rightarrow \Xi^0n$ ,  $\Lambda\Lambda$  transitions in nuclear medium, although it is difficult to determine the value of  $W_0^\Xi$  from the data due to the insufficient resolution of 14.7 MeV FWHM. The importance of the energy dependence of the Fermi-averaged  $K^-p \rightarrow K^+\Xi^-$  amplitude is confirmed by this analysis. The detailed analysis is also required for the J-PARC E05 experiment of the  ${}^{12}\text{C}(K^-, K^+)$  reaction at 1.8 GeV/ $c$  [5]. This investigation is a subject for future research.

### Acknowledgments

The authors thank Prof. T. Fukuda, Prof. T. Nagae, Prof. Y. Akaishi, Prof. S. Shinmura, and Dr. A. Doté for many valuable discussions and comments. This work was supported by

Grants-in-Aid for Scientific Research (KAKENHI) from the Japan Society for the Promotion of Science (Grant No. JP20K03954).

---

- [1] K. Nakazawa *et al.*, Prog. Theor. Exp. Phys. **2015**, 033D02 (2015).
- [2] T. Fukuda *et al.* (E224 Collaboration), Phys. Rev. **58**, 1306 (1998).
- [3] P. Khaustov *et al.* (The AGS E885 Collaboration), Phys. Rev. C **61**, 054603 (2000).
- [4] Y. Yamamoto, Few Body Syst. Suppl. **9**, 145 (1995); S. Tadokoro, H. Kobayashi, and Y. Akaishi, Phys. Rev. C **51**, 2656 (1995).
- [5] T. Nagae *et al.*, in *Proceedings of the 13th International Conference on Hypernuclear and Strange Particle Physics: HYP2018*, edited by L. Tang and R. Schumacher, AIP Conf. Proc. No. 2130 (AIP, New York, 2019), p. 020015.
- [6] D. Chatterjee and I. Vidana, Eur. Phys. J. A **52**, 29 (2016).
- [7] S. Balberg and A. Gal, Nucl. Phys. A **625**, 435 (1997).
- [8] M. Kohno, Phys. Rev. C **100**, 024313 (2019).
- [9] T. Tamagawa, Ph.D. Thesis, University of Tokyo, 2000 (unpublished).
- [10] T. Harada and Y. Hirabayashi, Phys. Rev. C **102**, 024618 (2020).
- [11] T. Harada and Y. Hirabayashi, Nucl. Phys. A **744**, 323 (2004).
- [12] O. Morimatsu and K. Yazaki, Prog. Part. Nucl. Phys. **33**, 679 (1994), and references therein.
- [13] J. Hüfner, S. Y. Lee, and H. A. Weidenmüller, Nucl. Phys. A **234**, 429 (1974).
- [14] E. H. Auerbach *et al.*, Ann. Phys. (N.Y.) **148**, 381 (1983).
- [15] C. B. Dover, L. Ludeking, and G. E. Walker, Phys. Rev. C **22**, 2073 (1980).
- [16] T. Harada and Y. Hirabayashi, Nucl. Phys. A **759**, 143 (2005); Nucl. Phys. A **767**, 206 (2006).
- [17] T. Harada, R. Honda, and Y. Hirabayashi, Phys. Rev. C **97**, 024601 (2018).
- [18] T. Harada and Y. Hirabayashi, Phys. Rev. C **100**, 024605 (2019).
- [19] S. Okabe, Y. Abe, and H. Tanaka, Prog. Theor. Phys. **57**, 866 (1977); S. Okabe and Y. Abe, Prog. Theor. Phys. **61**, 1049 (1979).
- [20] D. R. Tilley *et al.*, Nucl. Phys. A **708**, 3 (2002).
- [21] H. Tyrén *et al.*, Nucl. Phys. **79**, 321 (1966); G. Jacob and Th. A. Maris, Mod. Phys. **38**, 121 (1966); Rev. Mod. Phys. **45**, 6 (1973).
- [22] H. de Vries, C. W. de Jager, and C. de Vries, At. Data Nucl. Tables **36**, 459 (1987).

- [23] D. A. Sharov, V. L. Korotkikh, and D. E. Lanskoj, *Eur. Phys. J. A* **47**, 109 (2011), and references therein.
- [24] Y. Yamamoto and H. Bandō, *Phys. Lett. B* **214**, 173 (1988).
- [25] I. Tanihata, H. Savajols, and R. Kanungod, *Prog. Part. Nucl. Phys.* **68**, 215 (2013).
- [26] A. Bouyssy, *Nucl. Phys. A* **381**, 445 (1982).
- [27] A. Gal, G. Toker, and Y. Alexander, *Ann. Phys. (N.Y.)* **137**, 341 (1981).
- [28] J. Haidenbauer, U.-G. Meißner, and S. Petschauer, *Nucl. Phys. A* **954**, 273 (2016).
- [29] J. Haidenbauer and U.-G. Meißner, *Eur. Phys. J. A* **55**, 23 (2019).
- [30] K. Sasaki *et al.* (HAL QCD Collaboration), *Nucl. Phys. A* **998**, 121737 (2020).